Effect of stress state on deformation and fracture of nanocrystalline copper: Molecular dynamics simulation*

Zhang Liang(张 亮), Lü Cheng(吕 程)†, Kiet Tieu, Pei Lin-Qing(裴林清), and Zhao Xing(赵 星)

School of Mechanical, Materials and Mechatronic Engineering, University of Wollongong, Wollongong, NSW 2522, Australia

(Received 14 January 2014; revised manuscript received 12 March 2014; published online 16 July 2014)

Deformation in a microcomponent is often constrained by surrounding joined material making the component under mixed loading and multiple stress states. In this study, molecular dynamics (MD) simulation are conducted to probe the effect of stress states on the deformation and fracture of nanocrystalline Cu. Tensile strain is applied on a Cu single crystal, bicrystal and polycrystal respectively, under two different tension boundary conditions. Simulations are first conducted on the bicrystal and polycrystal models without lattice imperfection. The results reveal that, compared with the performance of simulation models under free boundary condition, the transverse stress caused by the constrained boundary condition leads to a much higher tensile stress and can severely limit the plastic deformation, which in return promotes cleavage fracture in the model. Simulations are then performed on Cu single crystal and polycrystal with an initial crack. Under constrained boundary condition, the crack tip propagates rapidly in the single crystal in a cleavage manner while the crack becomes blunting and extends along the grain boundaries in the polycrystal. Under free boundary condition, massive dislocation activities dominate the deformation mechanisms and the crack plays a little role in both single crystals and polycrystals.

Keywords: molecular dynamics, nanocrystalline, stress state, deformation mechanism

PACS: 81.07.Nb, 81.07.Bc, 81.40.Vw, 81.40.Jj **DOI:** 10.1088/1674-1056/23/9/098102

1. Introduction

Many nextgeneration microelectromechanical systems, nanoelectromechanical systems and other micro-devices have been studied, and they have been widely applied in the production practice, where the performance and reliability are contingent on the materials of which they are composed. Therefore, it is crucial to develop a sound understanding of deformation in materials with sub-micrometer dimensions. Compared with conventional coarser grained materials, nanostructure materials have a number of superior mechanical properties of potential significance for structure applications, including high yield and fracture strength,[1,2] superior wear resistance,[3–5] high fatigue resistance,[6–10] etc. The appealing mechanical characteristics of nanostructure materials have provoked great interest of researchers to explore its mechanical properties and underlying deformation mechanisms. Because the atomistic mechanisms are very hard to quantify experimentally, computer simulations based on atomistic models have become a powerful tool for gaining the fundamental knowledge in the past two decades and the results have been productive.

The properties and deformation mechanisms of nanocrystalline materials have been primarily studied with a focus on the impact of grain size.[11–19] The dislocation activities in the interior of grains lessen when the average grain size is less than 100 nm whereas the mechanisms mediated by the grain boundary become dominant. However, the grain size and the stress state can both dramatically influence the mechanical response of nanocrystalline materials.[20] For example, the hydrostatic pressure is determined to improve the plasticity of metal during the plastic forming process. Unfortunately, most of the previous research work conducted by atomistic simulations is under uniaxial tension or pure shear deformation, which is far from the actual situation where the micro or nanocomponents can be usually under mixed loading and multiple stress state. Very few authors have attempted to investigate the behavior and deformation mechanisms of nanocrystalline materials under multiple stress state at atomistic scale. Kitamura *et al.*[21] conducted numerical simulations to study the effect of transverse deformation on the fracture process of single-crystal nickel, the simulation results shown that the constraint placed on the boundaries transverse to the uniaxial loading direction can lead to very high tensile yield stresses and severely limit inelastic deformation. Warner and Molinari[22] used the molecular dynamics (MD) simulation to probe the influence of normal loading on grain boundary shear response. They reported that the shear strengths of some grain boundaries are correlated with normal stress acting on the interface. Spearot *et al.*[23,24] have recently examined a range of geometries of single crystal Cu and symmetric tilt grain boundaries loaded on tension, and thus, the stress state on the active slip system was indirectly varied as crystallographic orientation changed. They were able to shown that the non-glide direction stress components acting on the slip plane can influence the partial dislocation nucleation process and the maximum tensile

*Project supported by the Research Council Discovery Projects of Australia (Grant No. DP0773329).

†Corresponding author. E-mail: chenglu@uow.edu.au

© 2014 Chinese Physical Society and IOP Publishing Ltd

strength.

In this study, we conduct MD simulations to study the properties of deformation and fracture of nanocrystalline copper from the atomic point of view, both single crystal, bicrystal and polycrystal models are employed. Simulations are conducted firstly on a bicrystal and a polycrystal model without initial defects to investigate their mechanical properties and deformation behaviors. Then, a singlecrystal model and a polycrystal model with an initial crack are numerically simulated to study the propagation of crack. In order to create different stress states, tensile strain is added onto each model with two different boundary conditions. The details of simulation models and the boundary conditions will be described in Section 2. The simulation results are presented and discussed in Section 3.

2. Simulation method

2.1. Simulation model

Simulation models used in this study are presented in Fig. 1. The bicrystal model with a $\sum 5(310)$ grain boundary is created by constructing two separate crystals with different crystallographic orientation and joining them together along the Y axial (see Fig. 1(a)). The polycrystal model is generated by using the Voronoi construction method with random grain sizes and random crystallographic orientations (see Fig. 1(b)). It contains 27 grains with a mean grain size of 9.1 nm. The singlecrystal model is arranged routinely with its three crystallographic orientations along the X, Y, and Z coordinate axis, respectively. A wedgy crack is initially inserted into the side of the singlecrystal model (see Fig. 1(c)). The same polycrystal model of Fig. 1(b) with an initial crack is shown in Fig. 1(d). Periodic boundary conditions are applied along all directions (X, Y and Z) of the simulation models. It should be noted that the periodic boundary condition in the Y direction introduces a second boundary plane into the bicrystal model in Fig. 1(b). The initial crack in Figs. 1(c) and 1(d) can propagate on both sides of the models due to the periodic boundary condition in the X direction.

Simulation models are prepared by using combining molecular statics and MD simulations to obtain the equilibrium structures. Molecular statics calculations, which employ a nonlinear conjugate gradient method, are used to determine the minimum energy configurations. After that, the simulation model is equilibrated by using the MD simulations in a isobaric–isothermal (NPT) ensemble at a pressure of 0 bar and a temperature of 10 K for 20 ps. The dimension of the equilibrium models is given in Table 1. All the simulations in this study are performed with the LAMMPS code.[25]

The interatomic potential chosen for simulation plays a profound role in the accurate prediction of defective structures. In this study, Copper is modeled by using an embedded-atom method (EAM) potential developed by Mishin *et al.*[26] The intrinsic stacking fault energy and unstable stacking fault energy from simulation results are 44.4 mJ/m^2 and 158 mJ/m^2, respectively, which are very close to the experimental measurements (45 mJ/m^2 [27] and 162 mJ/m^2 [26]).

Table 1. Dimension of simulation models.

Simulation model	$X \times Y \times Z$/Å^3	Number of atoms
Bicrystal	$144.4 \times 218.4 \times 108.3$	285000
Polycrystal	$216.6 \times 216.6 \times 216.6$	832750
Single crystal with crack	$216.6 \times 216.6 \times 216.6$	850744
Polycrystal with crack	$216.6 \times 216.6 \times 216.6$	821367

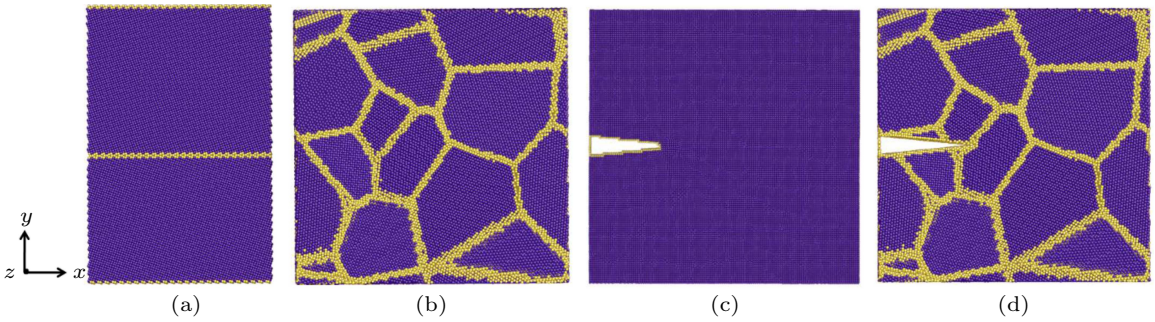


Fig. 1. (color online) Equilibrium configuration of simulation models. (a) Bicrystal model, (b) polycrystal model, (c) singlecrystal model with an initial crack, and (d) polycrystal model with an initial crack.

2.2. Boundary conditions of tensile loading

The simulation models are subjected to a tensile deformation along the Y direction at a constant strain rate of 1×10^9 s^{-1}. An integration time step of 1.0 fs is adopted throughout the MD simulations. The temperature is initially set at 10 K in every tension step to avoid the influence of the thermal motion of atoms at high temperature. In order to create different stress state, two different boundary conditions are used in this work. Specifically, MD simulations are performed using either "free" or "constrained" tension boundary conditions, as schemed in Fig. 2. For the free tension boundary condition, the boundaries in the lateral directions are allowed to expand or contract during the deformation process so that the transverse stress are kept free ($\sigma_{xx} = \sigma_{zz} = 0$), as shown

in Fig. 2(a). For the constrained tension boundary condition, computational models are strained at a constant rate along the Y axis while keeping the model dimensions fixed along the X and Z directions. The lateral boundaries are constrained by prevent the periodic simulation model from expanding or contracting during the deformation process ($\varepsilon_{xx} = \varepsilon_{zz} = 0$), as shown in Fig. 2(b). This boundary condition considers the transverse stress along the X and Z directions during the tensile deformation. The dashed lines in Fig. 2 represent the initial shape of the model, while the solid lines represent the deformed shape. These boundary conditions are very similar to those used by Kitamura *et al.*[21] and Spearot *et al.*[28] to study the effect of boundary condition on tensile deformation of nickel single crystal and copper bicrystal respectively.

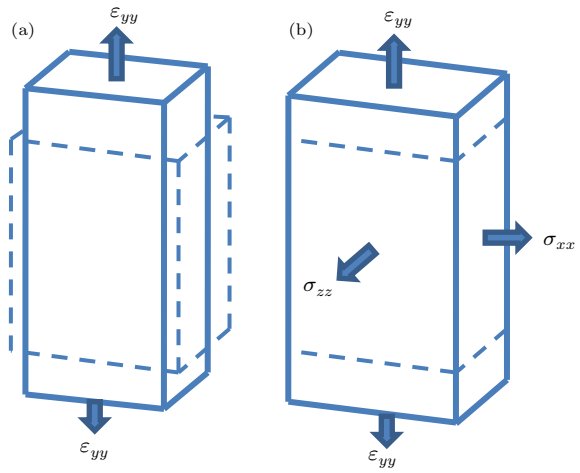


Fig. 2. (color online) Schematic of simulation models with two different tension boundary conditions: (a) free tension boundary condition, and (b) constrained tension boundary condition.[21]

In order to further validate the EAM potentials[26] and the MD code, simulations are designed to calculate the elastic stiffness (C_{11} and C_{12}) of Cu single crystal model. As introduced above, the displacement (or strain) in the X and Z directions is equal to zero under the constrained tension boundary condition. Thus, the following set of elastic equations that describe the response of a homogeneous cubic crystal:

$$\begin{bmatrix} \sigma_1 \\ \sigma_2 \\ \sigma_3 \\ \sigma_4 \\ \sigma_5 \\ \sigma_6 \end{bmatrix} = \begin{bmatrix} C_{11} & C_{12} & C_{12} & & & \\ C_{12} & C_{11} & C_{12} & & & \\ C_{12} & C_{12} & C_{11} & & & \\ & & & C_{44} & & \\ & & & & C_{44} & \\ & & & & & C_{44} \end{bmatrix} \begin{bmatrix} \varepsilon_1 \\ \varepsilon_2 \\ \varepsilon_3 \\ \varepsilon_4 \\ \varepsilon_5 \\ \varepsilon_6 \end{bmatrix} \quad (1)$$

reduces to

$$\sigma_1 = C_{12}\varepsilon_2 = \sigma_3, \quad (2)$$

$$\sigma_2 = C_{11}\varepsilon_2. \quad (3)$$

Thus, the elastic constants C_{11} and C_{12} can be determined by measuring the slope of an appropriate stress-strain relation. For the mechanical properties, the system stress is attained by calculating the pressure of the entire system of atoms. The pressure is calculated by

$$P_{ij} = \frac{1}{V}\left[\sum_k^N m_k v_{k_i} v_{k_j} + \sum_k^N r_{k_i} f_{k_j}\right], \quad (i, j = x, y, z), \quad (4)$$

where the first term uses components of the kinetic energy tensor and the second term uses components of the virial tensor. We define N as the total number of atoms in the simulation model, V the simulation model volume, r and f as the force vector and the distance vector respectively. System strain is derived from the positions of the periodic boundaries. The elastic constants calculated from the initial slope of the MD simulations are 173.2 GPa and 124.8 GPa, which are all within acceptable accuracy of the experimental values of 168.4 GPa and 121.4 GPa.[29]

In addition, only principle stress is applied in our study, as shown in Fig. 2. The well-established von Mises yield criterion can be described as follows:

$$\sigma_{\rm v} = \sqrt{\frac{1}{2}[(\sigma_1-\sigma_2)^2+(\sigma_1-\sigma_3)^2+(\sigma_2-\sigma_3)^2}. \quad (5)$$

In the case of free tension boundary condition ($\sigma_1 = \sigma_3 = 0$), the von Mises criterion simply reduces to

$$\sigma_{\rm v} = \sigma_2, \quad (6)$$

which means that the material starts to yield when σ_2 reaches the yield strength of the material $\sigma_{\rm v}$, and this is in agreement with the definition of tensile yield strength. On the other hand, in the case of constrained tension boundary condition ($\sigma_2 > \sigma_1 = \sigma_3 \neq 0$), the von Mises criterion can be expressed as

$$\sigma_{\rm v} = \sigma_2 - \sigma_1 = \sigma_2 - \sigma_3. \quad (7)$$

From Eqs. (6) and (7), we can deduce that the simulation model starts to yield at a higher tensile stress (σ_2) under the constrained boundary condition than the free boundary condition. Actually, this deduction is confirmed by our MD simulation in Section 3.

3. Simulation results

3.1. Tensile response of Cu bicrystal and polycrystal model

Figure 3 shows the tensile stress–strain response for Cu bicrystal model with a $\sum 5(310)$ grain boundary subject to a tensile deformation under two different tension boundary conditions. The maximum tensile stress corresponds to the nucleation of partial dislocations, in agreement with results for the uniaxial tensile of Cu bicrystal by Spearot *et al.*[30,31] The tensile stress required for dislocation emission of bicrystal model under constrained boundary condition is 13.47 GPa, which is significantly higher than that required under free boundary

condition (4.72 GPa). Apparently, the difference in the maximum tensile strength results from the stresses that are developed transversely to the loading direction during the deformation process. This result conforms to our deduction from the Mises yield criterion.

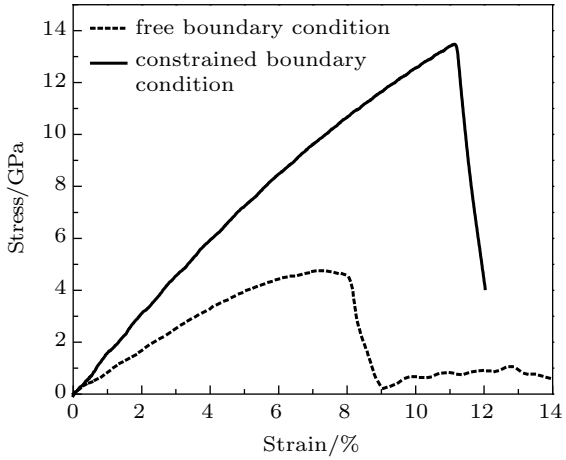


Fig. 3. Relationship between stress and strain of Cu bicrystal model under two different tension boundary conditions.

To gain fundamental understanding on the strength difference between two different tension boundary conditions, the deformation mechanisms at the atomistic scale are examined (see Figs. 4 and 5). The atomic mechanisms are determined by examining continuous snapshots stored during the MD simulation. All images are colored according to the common neighbor analysis (CNA) parameter.[32] Atoms with perfect fcc structures are removed to facilitate viewing of the defect structures. Atoms colored with yellow organize the grain boundary plane and the dislocation core, while the blue atoms correspond to the hcp structures that represent stacking faults.

Figures 4(a) and 5(a) show the snapshot of atoms in the bicrystal model at the beginning of the stress drop under the free boundary condition ($\varepsilon = 8\%$) and the constrained boundary condition ($\varepsilon = 11.2\%$) respectively. Images indicate that partial dislocations with both edge and screw characteristics are nucleated from the bicrystal interface once the maximum tensile stress is reached, regardless of whether free or constrained tension boundary condition is prescribed. In addition, the constrained boundary condition promotes the nucleation of crack along the grain boundary plane due to the local cleavage fracture at the stress drop, as shown in Fig. 5(b) at $\varepsilon = 11.8\%$. The crack propagates rapidly along the boundary plane and eventually results in the cleavage of the two grains of the bicrystal model. During the deformation process under the constrained boundary condition, a limited number of dislocations nucleate from the boundary plane that restricts the plastic deformation and cause the brittle behavior of the bicrystal model (as indicated by the sudden drop of the stress curve in Fig. 3). This is different from the case of the free boundary condition, where dislocation nucleation and propagation dominate the deformation mechanisms during the whole process of the simulation without any crack nucleation at $\varepsilon = 8.2\%$ (see Fig. 4(b)), or even at a higher strain rate (not shown here).

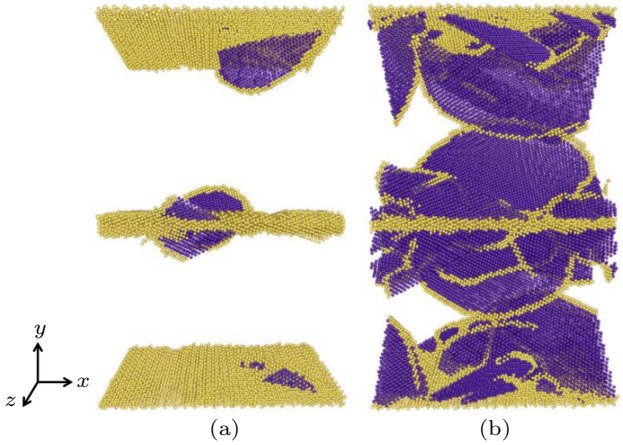


Fig. 4. (color online) Snapshots of copper bicrystal model at different tensile strain rate under free tension boundary condition at 10 K. (a) $\varepsilon = 8\%$ and (b) $\varepsilon = 8.2\%$.

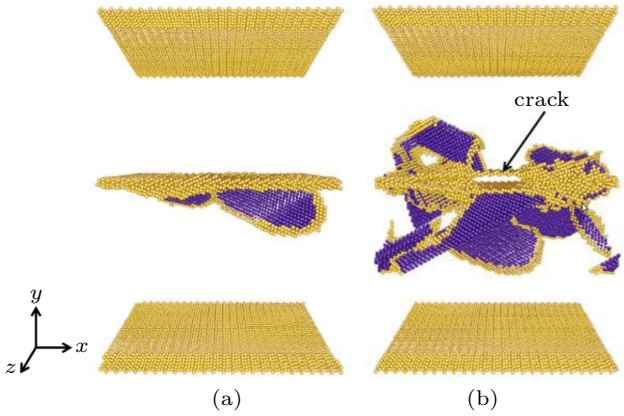


Fig. 5. (color online) Snapshots of copper bicrystal model at different tensile strain rate under constrained tension boundary condition at 10 K. (a) $\varepsilon = 11.2\%$, and (b) $\varepsilon = 11.8\%$.

The relationship between stress and strain of polycrystal Cu under two different tension boundary conditions is plotted in Fig. 6. Under the constrained boundary condition, the maximum tensile stress reaches 9.26 GPa much higher than the value under the free boundary condition (2.13 GPa) without the transverse stress, which conforms to our deduction from the Mises yield criterion. Figure 7 shows the atomic configuration of Cu polycrystal model at different tensile strain rate. Dark blue, yellow, and light blue atoms correspond to the local fcc, defect, and hcp structures classified by the CNA, respectively. Under the constrained boundary condition, some grain boundaries become coarser when the deformation is performed. Meanwhile, voids are nucleated along the grain boundaries after several dislocations have been emitted from the boundary plane at $\varepsilon = 5.5\%$ (see the snapshot of Fig. 7(b)). The nucleated voids grow and coalesce during the deformation

process eventually leading to complete fracture of the model. Recall that, the mechanical response and deformation mechanisms of Cu polycrystal under the constrained condition are quite similar to that described in Cu bicrystal model previously under the same condition.

The brittle behavior without obvious plastic strain under the constrained boundary condition is completely different from the ductile one under the free boundary condition where the slip deformation mechanism dominates the process. Massive dislocations nucleate from the grain boundary plane on one side, propagate across the grains and eventually are absorbed by the grain boundaries on the other side, leaving many stacking faults in the grains. The dislocation interaction also prevails in the Cu polycrystal, as shown in Fig. 7(a). This result is consistent with the previous simulation work on the Cu polycrystal model under a uniaxial tension[33–35] and in agreement with other fcc metals with low stacking fault energy in the experiments.[36,37] Note that no voids are nucleated during the tensile deformation under the free condition even at a high strain rate of $\varepsilon = 10\%$ (see Fig. 7(a)). The dislocation mediate deformation mechanism under the free boundary condition contributes to the ductile behavior of polycrystal Cu model and results in the stress flow in Fig. 6.

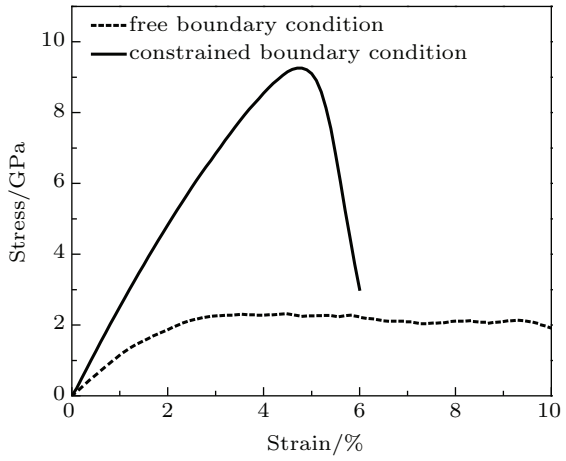


Fig. 6. Relationship between stress and strain of Cu polycrystal model under two different tension boundary conditions.

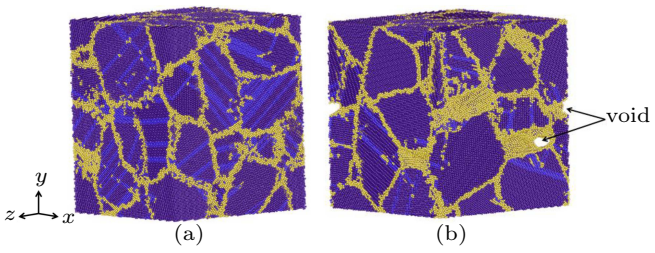


Fig. 7. (color online) Snapshots of the copper polycrystal model at different tensile strains under (a) free tension boundary condition and (b) constrained tension boundary condition at 10 K. (a) $\varepsilon = 10\%$; (b) $\varepsilon = 5.5\%$

3.2. Crack evolution in Cu single crystal and polycrystal

Figures 8 and 9 present the details of the atomistic process of the crack evolution in Cu single crystal under two different tension boundary conditions. In the case of free boundary condition, the initial crack-tip blunting occurs with the increase in the tensile deformation. However, the crack propagation is not obvious even when the tensile strain reaches $\varepsilon = 7\%$ (see Fig. 8(a)). There is a plastic region in front of the crack tip, and the atoms in this region are disordered rather than keep the initial fcc structure. The stress increases and then concentrates itself at the crack tip, resulting in the nucleation of dislocation in this region (see Fig. 8(a)). Note that the periodic boundary condition is applied on the X axis. As the applied strain increases, the crack blunting increases on both sides of the initial crack and consecutive dislocations are emitted from the crack frontier (see Figs. 8(b) and 8(c)).

Under constrained boundary condition, the crack propagates forward rapidly along the [1 0 0] direction, driven by something in a brittle manner. Atoms are still well ordered and no dislocation is emitted in the front of the crack tip at $\varepsilon = 5\%$ (see Fig. 9(a)). Crack propagation mechanisms involve only the fatigue cleavage of atomic bonds in the crack plane leading to crack extension. The plastic region appears at the crack frontier and dislocations nucleate on both sides of the crack at $\varepsilon = 6\%$ (see Fig. 9(b)), which is similar to the mechanism demonstrated in Fig. 8(b). However, different from the case of free boundary condition, in which dislocation nucleation and slipping accommodate the plastic deformation With the increase in the tensile strain, the crack keeps propagating forward in a cleavage manner and eventually results in the fracture of the model. Only a limited number of dislocations are nucleated during the tensile deformation.

It is worth noting that, the fracture of Cu single crystal in a brittle manner under constrained boundary condition is just one case since the single crystal model in this study is routinely arranged and the initial crack tip is inserted on the (001) plane. Actually, many deformation parameters should be taken into consideration when examining the brittle or ductile fracture mechanism in the simulation work, such as temperature, strain rate, shape of the created crack, oriented misorientation of grain atoms, the mode and value of applied force, etc. For example, Potirniche and coworkers[38] investigated the influence of crystallographic orientation on the crack growth path in single crystal Cu. In their MD simulation, the crack-tip plasticity is determined by the number of active slip systems resulting from different orientations. Both crack-tip blunting and fatigue cleavage were observed. In any case, the stress state is determined in our simulation as another significant factor that can affect the crack evolution in the bulk materials.

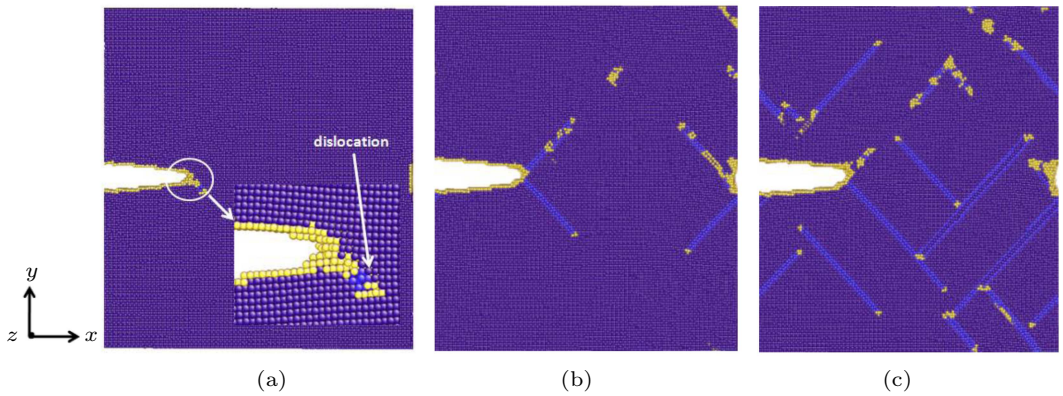


Fig. 8. (color online) Atomic configurations of cross sections of copper single crystal model with initial crack at tensile strain rates of (a) $\varepsilon = 7\%$, (b) $\varepsilon = 8.6\%$, and (c) $\varepsilon = 9\%$ under the free tension boundary condition at 10 K.

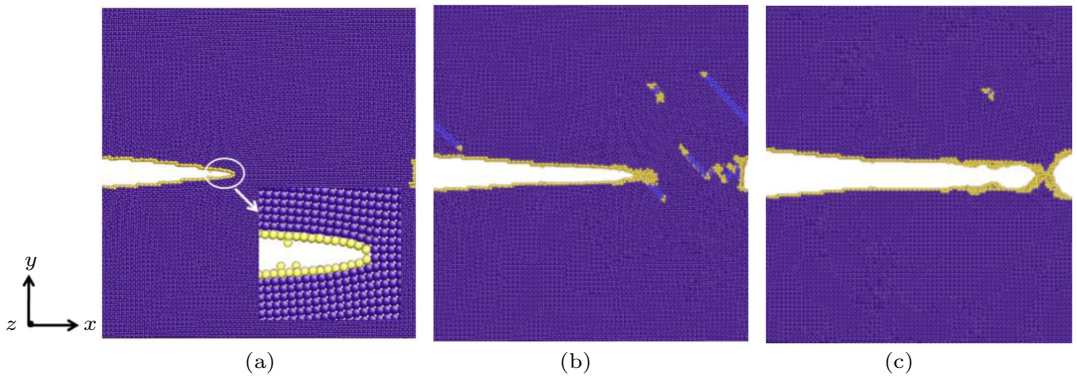


Fig. 9. (color online) Atomic configurations of cross sections of copper single crystal model with initial crack at tensile strain rates of (a) $\varepsilon = 5\%$, (b) $\varepsilon = 6\%$, and (c) $\varepsilon = 9\%$ under the constrained tension boundary condition at 10 K.

Figures 10 and 11 present the atomistic process of the crack evolution of polycrystal Cu under two tension boundary conditions. At $\varepsilon = 1\%$, crack keeps its original configuration under free boundary condition, some embryo partial dislocation nucleated from grain boundary near the crack-tip region in grain 1 (see Fig. 10(a)). With the increase in the applied tensile deformation, massive dislocations are emitted from the grain boundaries in each grain and travel through the grains to the opposite grain boundaries (see Fig. 10(b)). The initial inserted crack seems to play a little role during the deformation process since the crack tip does not propagate forward and no conspicuous crack blunting is observed in this case. Similar to the case of single crystal, dislocation mediated plastic deformation is the dominant mechanism of the Cu polycrystal under free boundary condition.

Under the constrained boundary condition, the crack becomes blunt compared with its initial configuration and propagates forward a small distance when the applied tensile strain reaches $\varepsilon = 1\%$ (see Fig. 11(a)). No embryo dislocation near the grain boundaries was observed in this stage. It is interesting that, with the increase in the tensile strain, the crack tip does not propagate forward in a brittle fracture manner as expected as its evolution in the singlecrystal model. Instead, the crack tip becomes significantly blunt and the crack extends along the neighboring grain boundaries. The intergranular fracture in this case is different from the intragranular fracture in our previous result,[39] which can be ascribed to the location of the initial crack. The crack tip in our previous simulation is arranged inside the grain and far from the nearest grain boundary. While in this work, the crack tip is inserted at the grain boundary place (see Fig. 1(d)). Comparing the crack performance of the polycrystal model with that of the single-crystal model under the constrained boundary condition (also with our former simulation results), we reach two conclusions: 1) the crystallographic orientation of grain on the crack growth path has a strong impact on the crack propogation; and 2) the grain boundary is the preferential path of the crack extension since the atoms on the boundary plane have higher energy and are easier to diffuse.

In addition, massive dislocations are observed in a polycrystal Cu under the constrained boundary condition at $\varepsilon = 8\%$. Note that, under the free boundary condition, dislocations are first nucleated from one side of each grain and then propagate along the same slip plane to the opposite side (see Fig. 10(b)). However, under the constrained boundary condition, the transverse stress activates more slip systems so that dislocations can be nucleated from different grain boundaries in each grain and slip on different slip planes (see Fig. 11(b)).

The propagation of dislocations on different slip system can induce relative sliding between two neighboring grains,[35] and a grain rotation occurs as a result of cooperative sliding along the opposite boundaries of the grain. For example, grain 1 and grain 2 in Fig. 11(a) have different crystallographic orientation at $\varepsilon = 1\%$, but the relative rotation of the two grains changes their initial orientation gradually eventually resulting in the combination of the two grains at $\varepsilon = 8\%$ (see Fig. 11(b)). Moreover, the rotation of grains can also lead to the separation of the grain, the grain 3 splits into two grains at $\varepsilon = 8\%$ (see Fig. 11). The grain rotation induced grain separation or combination are not observed in other grains of the polycrystal at $\varepsilon = 8\%$. This happens mainly because that small grains rotate much faster than larger ones.[35] Furthermore, the grain boundary migration, which has been reported,[40,41] is not obvious at $\varepsilon = 8\%$ under both of the two tension boundary conditions. This is mainly attributed to the low temperature, and the fact that the accumulated local stress may not be high enough to drive the motion of the grain boundaries.[42,43]

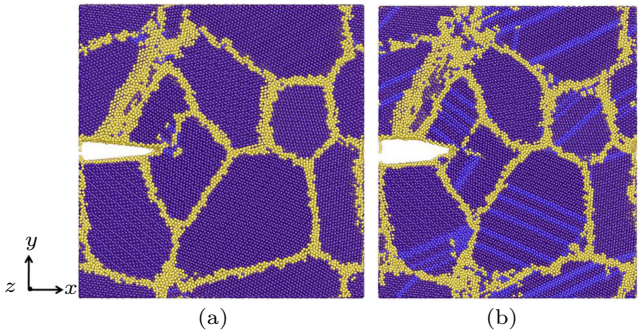


Fig. 10. (color online) Atomic configurations of cross sections of the copper polycrystal model with an initial crack at tensile strain rates of (a) $\varepsilon = 1\%$ and (b) $\varepsilon = 8\%$ under the free tension boundary condition at 10 K.

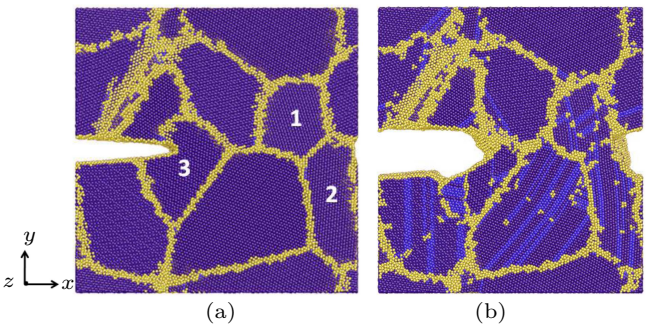


Fig. 11. (color online) Atomic configurations of cross sections of the copper polycrystal model with an initial crack at tensile strain rates of (a) $\varepsilon = 1\%$ and (b) $\varepsilon = 8\%$ under the free tension boundary condition at 10 K.

4. Conclusions

The mechanism of deformation and fracture of Cu single crystal, bicrystal and polycrystal has been studied at the nanoscale under two different tension boundary conditions using MD simulations. We demonstrate that the stress state is particularly important in determining mechanical properties and fatigue resistance in materials. The results are summarized as follows.

(i) For the Cu bicrystal and polycrystal models, the tensile stress required for dislocation emission for the bicrystal and polycrystal under the constrained boundary condition are significantly higher than that required under free boundary condition. The failure of models is dominated solely by partial dislocation slip activity under the free boundary condition; while under constrained boundary condition, the multistate of tensile stress due to the transverse stress perpendicular to the tensile axial leads to a more brittle mode of failure.

(ii) The evolution of crack in the Cu singlecrystal model under two tension boundary conditions are completely different. Under free boundary condition, the emission of dislocations from the crack tip and their propagation are the dominant mechanisms during the tensile deformation. The deformation mechanism is quite another thing under the constrained boundary condition, where the crack extends along the [1 0 0] direction in a cleavage manner and eventually results in the fracture of the model.

(iii) Under the free boundary condition, the crack plays a little role during the tensile deformation of Cu polycrystal in this study, dislocation nucleation from the grain boundary and its propagation in the grain are the dominant mechanism. Under the constrained boundary condition, grain boundaries hinder the propagation of the crack tip but provide the path for the extension of the crack. In addition, the principle tensile stress along with the transverse stress can activate multiple slip systems in each grain of the Cu polycrystal.

Acknowledgments

Simulations in this work were performed by using the HPC cluster of University of Wollongong and the computing facilities provided by the NCI National Facility of Australia. L. Zhang, L. Q. Pei and X. Zhao would like to acknowledge the financial support from the China Scholarship Council (CSC).

References

[1] Dao M, Lu L Asaro R J, de Hosson J T M and Ma E 2007 *Acta Mater.* **55** 4041
[2] Weertman 1999 *MRS Bull.* **24** 44
[3] Farhat Z N, Ding Y, Northwood D O and Alpas A T 1996 *Mater. Sci. Eng. A* **206** 302
[4] Jeong D H, Gonzalez F, Palumbo G, Aust K T and Erb U 2001 *Scr. Mater.* **44** 493
[5] Rupert T J and Schuh C A 2010 *Acta Mater.* **58** 4137
[6] Hanlon T, Tabachnikova E D and Suresh S 2005 *Int. J. Fatigue* **27** 1147
[7] Cavaliere P 2009 *Int. J. Fatigue* **31** 1476
[8] Xie J J and Hong Y S 2009 *Acta Metall. Sin.* **45** 844
[9] Wang Y B, Zhang G, Liu M J, Chen X L and Chen J 2009 *Chin. Phys. B* **18** 1181
[10] Xie S F, Chen S D and Soh A K 2011 *Chin. Phys. Lett.* **28** 066201

[11] Wolf D, Yamakov V, Phillpot S R, Mukherjee A and Gleiter H 2005 *Acta Mater.* **53** 1
[12] Schiotz J, Di Tolla F D and Jacobsen K W 1998 *Nature* **391** 561
[13] van Swygenhoven H, Spaczer M, Caro A and Farkas D 1999 *Phys. Rev. B* **60** 22
[14] van Swygenhoven H, P M Derlet 2001 *Phys. Rev. B* **64** 224105
[15] Yamakov V, Wolf D, Salazar M, Phillpot S R and Gleiter H 2001 *Acta Mater.* **49** 2713
[16] van Swygenhoven H, Derlet P M and Frøseth A G 2006 *Acta Mater.* **54** 1975
[17] Sansoz F and Molinari J F 2005 *Acta Mater.* **53** 1931
[18] Zhou Y M, He Y G, Lu A X and Wang Q 2009 *Chin. Phys. B* **18** 3966
[19] Wang T, Zhou F X and Liu Y W 2001 *Chin. Phys. Lett.* **18** 1242
[20] Sutton A P and Balluffi R W 1995 *Interfaces in Crystalline Materials* **p.** 205
[21] Kitamura T, Yashiro K and Ohtani R 1997 *JSME Int. J. Ser. A* **40** 430
[22] Warner D H and Molinari J F 2008 *Model. Simul. Mater Sci. Eng.* **16** 705
[23] Spearot D E, Tschopp M A, Jacob K I and McDowell D L 2007 *Acta Mater.* **55** 7507
[24] Tschopp M A and McDowell D L 2007 *Appl. Phys. Lett.* **75** 121916
[25] Plimpton S 1995 *J. Comput. Phys.* **117** 1
[26] Mishin Y, Mehl M J, Papaconstantopoulos D A, Voter A F and Kress J D 2001 *Phys. Rev. B* **63** 2241061
[27] Carter C B and Ray I L F 1977 *Philos. Mag.* **35** 189
[28] Spearot D E 2008 *Mech. Res. Commun.* **35** 81
[29] Hertzberg R W *Deformation and Fracture Mechanics of Engineering Materials* (New York: Wiley & Sons)
[30] Spearot D E, Jacob K I and McDowell D L 2007 *Int. J. Plasticity* **23** 143
[31] Tschopp M A and McDowell D L 2008 *Int. J. Plasticity* **24** 191
[32] Schiøtz J, Di Tolla F D and Jacobsen K W 1998 *Nature* **391** 561
[33] van Swygenhoven H and Weertman J R 2006 *Mater. Today* **9** 24
[34] Shimokawa T, Nakatani A and Kitagawa H 2004 *JSME Int. J. Ser. A* **47** 83
[35] Zheng Y G, Zhang H W, Chen Z, Lu C and Mai Y W 2009 *Phys. Lett. A* **373** 570
[36] Kizuka T 1998 *Phys. Rev. B* **57** 11158
[37] Furuya K, Mitsuishi K, Ishikawa N and Allen C W 2000 *Mater. Sci. Eng. A* **285** 85
[38] Potirniche G P, Horstemeyer M F, Gullett P M and Jelinek B 2006 *Proc. R. Soc. A* **462** 3707
[39] Qing P L, Cheng L, Kiet T, Tao Z H, Xing Z, Yu C K and Liang Z 2013 *J. Nano. Res.* **25** 188
[40] Legros M, Gianola D S and Hemker K J 2008 *Acta Mater* **56** 3380
[41] Merkle K L, Thompson L J and Phillipp F 2004 *Interface Sci.* **12** 277
[42] Haslam A J, Moldovan D, Yamakov V, Wolf D, Phillpot S R and Gleiter H 2003 *Acta Mater.* **51** 2097
[43] Shiga M and Shinoda W 2004 *Phys. Rev. B* **70** 054102